

## COMPUTATIONAL MODELLING OF HEAD-RELATED TRANSFER FUNCTION

Andrzej B. DOBRUCKI, Przemysław PLASKOTA

Wrocław University of Technology  
Institute of Telecommunications, Teleinformatics and Acoustics  
Wybrzeże Wyspiańskiego 27, 50-370 Wrocław, Poland  
e-mail: andrzej.dobrucki@pwr.wroc.pl

*(received May 21, 2007; accepted July 20, 2007)*

Measuring the Head-Related Transfer Function (HRTF) is an efficient method that takes into consideration the influence of the human body on the sound spectrum. The data base used in reproduction of the sound source position is built using the measurement results. The base is individual for each person, which makes it impossible to make a versatile base for all listeners. In this paper a numerical model of artificial head is presented. The model allows to determine the value of HRTF without making measurements. The model includes both geometrical and acoustical parameters. A method which is often used to determine the acoustical field parameters is the boundary element method, which was used to calculate the values of HRTF in this work. In the conclusion results of the calculations are presented and the correctness of the previous assumption made while constructing the geometric part of the numerical human head model is discussed.

**Keywords:** spatial hearing, Head Related Transfer Function, Boundary Element Method.

### 1. Introduction

In recent years surround sound systems have become widespread. The effect of surrounding the listener with sound is achieved by exploiting acoustic phenomena having a bearing on sound source localization. Similarly as in stereophony, the time, intensity and phase dependencies of signals arriving from individual sound sources are exploited. In addition, the influence of the acoustic system formed by the pinna, the head and the torso on the sound frequency response is taken into account. This influence is described by the Head-Related Transfer Function (HRTF). The knowledge about the influence of the human body structural features on the perception of sound source location in space is increasingly often applied in building sound systems.

So far, the best way of taking into account the effects of the human body on the sound frequency response is to measure HRTF for different sound source locations rel-

ative to the listener. The acquired measurement results form a database which is used in sound reproduction. It is difficult to create a proper HRTF database since each person has unique body structural features whereby it is impossible to create a universal database for all listeners. Therefore the use of the knowledge about the influence of the human body structure on the sound frequency response is difficult. In order to take such parameters into account one must carry out painstaking measurements for each person.

This paper's primary objective is to build a numerical model of the human head. The model will make it possible to calculate HRTF without the need to perform measurements. The model is created primarily to run simulations depicting the human head's influence on sound parameters. The model's design should allow one to take into account different geometric shapes of the human head, particularly of the pinna, and changes in other parameters, e.g. in the acoustic impedance of the skin. Numerical computations of acoustic wave propagation carried out using the numerical head model are to prove the validity of the latter.

Several major factors having a bearing on sound source localizability are distinguished. The two principal phenomena associated with sound source localization are: the Interaural Level Difference (ILD) and the Interaural Time Difference (ITD) [2]. But in the space surrounding the listener there are points for which the above factors are not explicit. Thus it is necessary to describe other factors affecting sound source localization. One of such factors is the Head-Related Transfer Function (HRTF).

HRTF is a representation of the influence of the acoustic system formed by the pinna, the head and the human torso on the deformation of the acoustic signal spectrum reaching the listener's ear. The head's shape and tissue material structure have a bearing on acoustic signal spectrum distortion. Thanks to changes in the spectrum the listener is able to more accurately localize the sound source in the space which surrounds her/him. In the case of headphone listening the influence of the acoustic system formed by the pinna, the head and the human torso is eliminated whereby the acoustic signal received by the listener is unnatural – the listener localizes the sound source inside her/his head. Through the use of HRTF measurement results the signal can be so deformed that the listener subjectively identifies the spatial properties of the sound whereby the location of the sound source in the space surrounding the listener is reproduced [13, 22, 24, 26]. Since there are many sound source locations in the space surrounding the listener many HRTFs are needed to accurately reproduce the location of the sound source in this space.

The function describing the direction-dependent acoustic filtering of sounds in a free field by the head, the torso and the pinna is called HRTF. Although it is obvious that the linear dependence between ITD, ILD and the perceived location in space needs to be predicted, it is less obvious how the spectral structure and the location in space can be mathematically interrelated [6]. The first step towards understanding the significance of the signal spectrum in directional hearing was an attempt at physical modelling and empirical measurement, followed by computer simulations of the ear's frequency response depending on the direction. The measured frequency response of the ear is subject to further analysis. This is schematically shown in Fig. 1.



Fig. 1. Block diagram defining head-related transfer functions:  $S(f)$  – measurement signal,  $H(f)$  – sought HRTF,  $M(f)$  – signal measured at entrance into aural canal.

Formally, a single HRTF is defined as a frequency response peculiar to the right or left ear frequency response, measured in a given point of the ear canal. The measurement takes place in the far field of a sound source located in the free field. Typical HRTFs are measured for the two ears at a fixed distance from the listener's head for a few different spatial locations. Thus the head-related transfer function depends on the azimuthal angle,  $\theta$ , the elevation angle,  $\phi$  and the frequency; its value is different for the left ear (L) and the right ear (R):  $\text{HRTF}_{L,R}(\theta, \phi, f)$ . The HRTF equivalent in the time domain is a Head-Related Impulse Response (HRIR).

The schematic shown in Fig. 1 is simplified. In reality the transfer function measured in this way includes a certain constant factor. The latter represents the measurement conditions – the measurement room response and the measurement path response. The parameter is a reference response whose value is determined by measuring the impulse response without the presence of the measured object. Hence, taking into account the reference response, the transfer function measurement result can be written as

$$h_{L,R}(\theta, \varphi, t) = s(t) * c(t) * \text{HRIR}_{L,R}(\theta, \varphi, t), \quad (1)$$

where  $h_{L,R}(\theta, \varphi, t)$  – the impulse response at the entrance to the auditory canal,  $\theta$  – the azimuthal angle,  $\varphi$  – the elevation angle,  $s(t)$  – the measurement signal,  $c(t)$  – the impulse response of the measuring circuit,  $\text{HRIR}_{L,R}(\theta, \varphi, t)$  – the head-related impulse response,  $*$  – the convolution operation.

Under certain conditions one can assume that  $c(t)$  is independent of the measuring point location in space. Then  $c(t)$  is an average of measurement results for several different azimuthal angles and elevation angles [6]. If, however, the measurement room does not satisfy the anechoic chamber conditions or there are elements in it which cause undesirable reflections, then factor  $c(t)$  is determined by both time and the location of the measuring point in the space surrounding the listener, but it is different for the left and right ear:  $c_{L,R}(\theta, \phi, t)$ . In order to increase measurement accuracy one can measure  $c_{L,R}(\theta, \phi, t)$  for each measuring point and then take into account the values during the processing of the measurement results.

Equation (1) can also be written in the frequency domain:

$$H_{L,R}(\theta, \varphi, f) = S(f) C(f) \text{HRTF}_{L,R}(\theta, \varphi, f), \quad (2)$$

Then HRTF is calculated from:

$$|\text{HRTF}_{L,R}(\theta, \varphi, f)| = \frac{|H_{L,R}(\theta, \varphi, f)|}{|S(f)| |C(f)|}, \quad (3)$$

$$\arg \text{HRTF}_{L,R}(\theta, \varphi, f) = \arg H_{L,R}(\theta, \varphi, f) - \arg S(f) - \arg C(f), \quad (4)$$

$$\text{HRTF}_{L,R}(\theta, \varphi, f) = |\text{HRTF}_{L,R}(\theta, \varphi, f)| \exp [j \arg \text{HRTF}_{L,R}(\theta, \varphi, f)], \quad (5)$$

and HRIR from:

$$\text{HRIR}_{L,R}(\theta, \varphi, t) = \mathcal{F}^{-1} [\text{HRTF}_{L,R}(\theta, \varphi, t)], \quad (6)$$

where:  $\mathcal{F}^{-1}$  – is the inverse Fourier transform.

The most suitable shape for the numerical model is a real object. Two types of objects: a human listener or an artificial head are available. It makes sense to first use an artificial head for numerical calculations owing to its simple shape, lower parameter variation and ease of measurement [17, 19, 21].

The geometric shape of the artificial head shown in Fig. 2 takes into account the most important morphological parameters such as: length, width and face width and omits unimportant details. Whereas the head's outer ear includes all the actual morphological components.



Fig. 2. Dummy head KU 100.

A numerical model of the head consists of two main parts, one of which describes the object's geometry while the other describes the acoustic impedance of the model's surface. The methods of creating the geometric part and the impedance part can be easily applied to the human head. In the case of the geometric part one must additionally make a cast of the head. Thus the methods are universal. The next sections show how to create the model's two parts for dummy head KU 100.

## 2. Modelling head and ear geometry

### 2.1. Geometric model of the head

The model was made in collaboration with the Institute of Production Engineering and Automation at Wrocław University of Technology. The Renishaw CYCLONE scanning system was used to make the model. The system allows one to scan three-dimensional objects. It is used to produce documentation for objects whose documentation for some reasons does not exist. 3-D models are created on the basis of a cloud of points. Then the models can be converted into detailed drawings.

The device works with two kinds of scanning heads: a contact head and a laser head. The kind of scanning head is chosen depending on the required accuracy and the material from which the specimen is made. Because of the peculiar shape of the KU 100 dummy head it was necessary to use the contact scanning head. The placement of the whole investigated object in the measuring device is shown in Fig. 3.

The measurement result is a cloud of points (Fig. 4). Only through further processing, e.g. by imposing a mesh of triangles, one can obtain a surface. Thanks to such processing the model can be later imported into a program in which a model suitable for work with a sound field determining program is created.

In the next step the individual points are connected so as to obtain a set of triangles (Fig. 5). The planes bounded by the sides of the triangles approximate the shape of the



Fig. 3. Dummy head KU 100 in 3-D scanner holder.

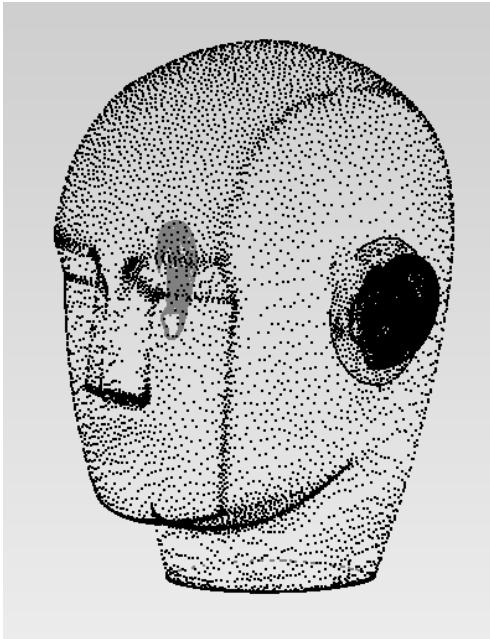


Fig. 4. Cloud of points – result of object measurement by means of 3-D scanner.

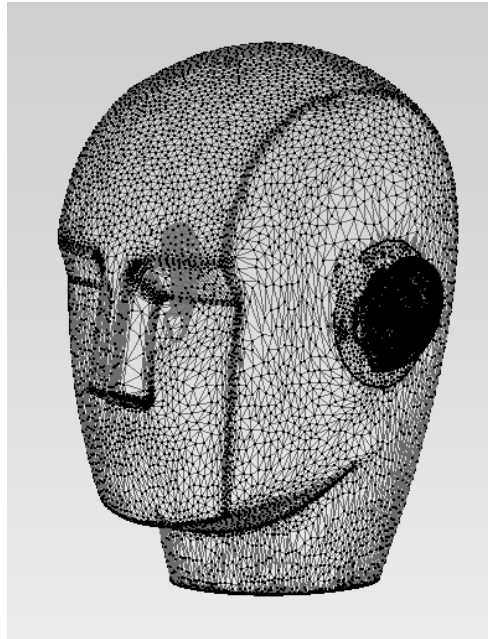


Fig. 5. Cloud of points connected by segments.

real object. It is apparent that as the number of triangles is increased the shape of the surface is better approximated. The size and number of triangles is particularly critical at places where the shape of the surface changes sharply, e.g. on the edges. The size of individual elements affects the accuracy of calculations performed using numerical methods (FEM, BEM) which will be employed later in this paper. When creating the geometric model it was assumed that the element size should be such as to ensure model validity for frequencies much exceeding the range of audio frequencies. In order for the model to satisfy the numerical calculation accuracy requirements the number of elements will be reduced in the next stage of work on the model.

The geometric model of the ear and the geometric model of the head were made separately and so combining the pinna model with the head model posed an additional difficulty. In order to ensure the validity of the whole model the two components should be so combined as to preserve their mutual geometry. For this purpose the 3-D scanner was used to determine control points on the head's and the ear's surface. The points helped to combine the two models with proper precision.

## 2.2. Geometric model of the ear

It is not possible to apply the methods described in the section on the geometric model of the head to create a geometric model of the ear. This is mainly due to the complicated shape of the pinna. The small hollows make it impossible to use the 3-D

scanner's contact head. Some hollows in the pinna have a diameter smaller than the scanning head's diameter. Since the diameter is about 4 mm, the scanning head is unable to accurately map, for example, grooves whose width is smaller than the scanning head's size. The obstacle to the use of the laser scanning head is on one hand the too low reflection coefficient and on the other hand the laser beam does not reach the surfaces located under other surfaces. Also the so-called negative angles, i.e. concavities, pose a problem.

In order to map the geometric shape of the pinna it is necessary to scan its cross-sections. The scanned cross-sections are then used to build a 3-D model, similarly as in dental prosthetics. The model is created as follows. First a silicone negative of the modelled pinna is made. The silicone mould is then used to make a plaster positive of the pinna. Gypsum with increased hardness is most suitable for this purpose. It has very good plastic properties and in addition it can be worked using abrasive tools. The positive is filled with contrastingly coloured plaster in such a way as to obtain a 3-D solid in the form of a cuboid. For further working it is important that the cast's opposite walls be parallel.

The next step in the creation of the model consists in sectioning the cast and scanning the cross-sections. The individual layers are best cut off using numerically controlled tools whereby very high precision of model mapping is achieved – the individual cross-sections must be spaced at every 0.1 mm. Each cross-section is then scanned by an optical scanner and in this way a digital image of the plaster cast is obtained.

Then the pinna cross-sections in the form of vector graphics are inserted into the Raindrop Geomagic Studio program for modelling 3-D solids. The individual cross-sections are stacked in a proper order, maintaining the same spacing as during the sectioning. The program operator indicates how the cross-sections are to be covered with planes. The planes are not homogenous, consisting of polygons, e.g. triangles. The geometric model of the ear obtained in this way is very precise and includes all the shapes of the real object.

### 2.3. Model reduction

The numerical calculations were performed using the Sysnoise software package for the numerical modelling of the acoustic field. One of the software's basic requirements is that a model be compatible with the input format.

The original model consists of 75 672 elements which are nonuniformly distributed, i.e. much more densely around the pinnas than on the rest of the head's surface. The differences are due to the ways in which the particular areas are modelled. It is important that the element size be proper for the frequency range for which the calculations will be performed. It is assumed [16] that the model is correct for the frequency range in which the dimensions of the largest element  $l_{\max}$  are smaller than 1/6 of the wavelength:

$$f_{\max} \leq \frac{c}{6 \cdot l_{\max}}, \quad (7)$$

where  $c$  – sound speed.

The absolute minimum is 4 linear elements per wavelength, in which case the acoustic field estimation error increases [3, 8].

Table 1 shows model upper limit frequencies depending on the number of model elements. The original model is characterized by a large frequency dispersion, i.e. the frequency for which all the elements satisfy condition (7) is low and the frequency for which 20% of the elements satisfy this condition is high. As a result of further modifications of the model this disproportion was reduced.

**Table 1.** Model upper limit frequencies depending on number of elements for 6 element lengths per wavelength.

		Number of model elements		
		139098	75672	11060
Number of elements satisfying condition (7)	100%	11.33 kHz	1.69 kHz	4.36 kHz
	80%	16.33 kHz	12.95 kHz	5.67 kHz
	60%	19.81 kHz	31.42 kHz	6.97 kHz
	40%	24.24 kHz	48.33 kHz	9.42 kHz
	20%	51.52 kHz	71.39 kHz	14.11 kHz

The large frequency dispersion is due to the fact that in the original model there is a large disproportion between the number of elements in the particular areas of the model. The 75 672 elements comprise 28 092 elements which describe the head's shape and 47 580 elements describing the shape of the pinnas. Thus the shape of one pinna is described by 23 790 elements, i.e. by about 85% of the number of elements which describe the shape of the head. The overall proportion is as follows: 37% of the elements describe the head while 63% of the elements describe the shape of the pinnas.

The analysis presented in Table 2 is carried out by selecting from 20% to 100% of the smallest model elements in the successive steps (of course, all the elements are taken into account in the final step). In the case of a model consisting of 75 672 elements, 20%, 40% and 60% of the smallest elements are elements which describe exclusively the shape of the pinnas. Since the pinna elements are small in comparison with the head elements, the limit frequency which follows from relation (7) is relatively high and much exceeds the range of frequencies perceived by the human being. On the other hand, there are relatively large elements among the head elements. It is a small set of a few dozen elements characterized by a high height/width ratio. These elements are located in places where the surface curvature is slight. Due to the presence of such elements the whole model has a relatively low limit frequency of about 1.7 kHz.

The optimization procedure consists in reducing the disproportion between the number of elements describing the shape of the pinnas and the number of elements describing the head. When the number of elements is to be increased, the largest elements are divided into smaller ones. In this case, the model's shape does not change since the new smaller elements are located within the surfaces of the elements that are divided.

**Table 2.** Maximum frequencies for which model is correct, depending on assumed number of elements per wavelength.

		Number of linear elements per wavelength		
		6	5	4
Number of elements satisfying condition (7)	100%	4.36 kHz	5.23 kHz	6.54 kHz
	80%	5.67 kHz	6.81 kHz	8.51 kHz
	60%	6.97 kHz	8.36 kHz	10.45 kHz
	40%	9.42 kHz	11.30 kHz	14.13 kHz
	20%	14.11 kHz	16.93 kHz	21.17 kHz

When the number of elements is to be reduced, the problem is more complicated since the reduction of the number of elements introduces a certain shape mapping error. The new larger elements are the resultants of a few smaller elements. The next optimization step consists in eliminating long, narrow elements which lower the model's limit frequency, by dividing each such element into several smaller ones.

Then two operations were performed. The first consisted in dividing the element grid so as to obtain the highest frequency for which condition (7) is satisfied. For this purpose the largest elements, i.e. the ones describing the head, were selected. The result was a model consisting of 139 098 elements, i.e. nearly twice as large as the original. The model's upper limit frequency is about 11.3 kHz, which means that the model covers the whole frequency range in which significant localization factors occur. But it turned out that this model could not be used for numerical calculations because of the computation time. The computation of acoustic field distribution for a single frequency would take about 170 hours, i.e. about 7 days. The computation of HRTF for a frequency range of 1–10 kHz with a resolution of 200 Hz for a single sound source location in space would take about 345 days. Therefore it was obvious that the model could not be used in further research.

It became necessary to work out a compromise between computation time and the number of elements satisfying condition (7). The number of elements was reduced mainly by reducing the number of elements describing the pinna. The result was a model consisting of 11 060 elements. The greater density of elements describing the pinna, in comparison with other areas of the model, was preserved in order not to change the shape significantly (the shape could change maximally by 0.4 mm). The important thing was to maintain the greatest finite element mesh density around the system response measurement point and this conditions was satisfied [1, 4]. The model has a higher limit frequency ( $f_{\max} = 4360$  Hz) than the original model.

In the next step the model's validity depending on the number of elements per wavelength was analyzed. Table 2 shows the results of the analysis. It follows from them that for four elements per one wavelength the model is correct up to the frequency of about 6.5 kHz. Also, considering that the pinnas are described by a larger number of elements

than the rest of the model, it can be assumed that the model is certainly correct up to the frequency of 7 kHz. But as the number of elements per wavelength is reduced the numerical calculation error increases. On the other hand, condition (7) applies to a situation in which all the elements are of the same or similar size. In the head model there are very few elements having a similar shape and the location of the elements is highly irregular. The particular element edges actually do not form straight lines. Thus one can say that there are no cases in which the dimension of six adjoining elements exceeds the length of the acoustic wave described by the upper limit frequency. This is another reason for recognizing the validity of the model above the frequency of 4.3 kHz.

It is also necessary to determine the lower limit frequency of the range for which numerical computations will be performed. Since the lower limit frequency of the device measuring HRTF is 200 Hz it is justified to adopt this frequency as the bottom limit frequency used for the numerical calculation of HRTF.

The boundary conditions assignable to the head model were analyzed. A simulation for the rigid model was the obvious thing to do. No impedance boundary conditions means that the Neumann boundary condition is the boundary condition and the assigned acoustic velocity is  $v_n = 0$ . Another model for which numerical calculations should be done is the model with assigned impedance boundary conditions. The assigned acoustic impedance value is consistent with the measurement results presented in Sec. 3. The acoustic impedance was assigned to the whole area, even though it is a value representing the materials used to make the body of the artificial head. The pinnas are made of material with a slightly different shell structure, but it is still rubber. Therefore in the first approximation one can assume that the acoustic impedance value is the same as for the other parts of the artificial head.

In order to find out if the acoustic impedance of the pinnas has a significant influence on the result of numerical calculations a different impedance than the one assigned to the rest of the head was assigned to the pinnas. A measured acoustic impedance was assigned to the head area while the area of the pinnas remained rigid. The rigid area is covered exclusively by the pinna's part sticking out of the head's outline. In a real head the pinna is integrated with a certain additional area. In order to find out if the area adjacent to the pinna has a significant influence on the result of numerical calculations, the simulations for the model in which the rigid area is enlarged and covers a part of the head adjacent to the pinna were run.

The numerical calculations showed that if the pinna is left as a rigid element this significantly affects the results (see Fig. 11). Then it was investigated whether the enlargement of the rigid area around the pinna affects the result of numerical calculations. It turned out that in this case the change of values is slight and the differences in the calculated responses are not larger than 0.2 dB.

Ultimately, numerical calculations for the whole space surrounding the listener were done for three models: the rigid model, the model with acoustic impedance assigned to the whole area and the model in which the rigid area covers the pinna together with the adjacent area. The sound sources used in the model were located at a distance of 1 m from the model, i.e. at the same distance as during the measurement of transfer

function for the actual object. Point sound sources with an omnidirectional radiation characteristic were employed. An identical sound source acoustic pressure amplitude, i.e. 1 Pa, was fixed for the whole frequency range.

It was tested whether the response of the investigated acoustic system is different depending on whether a sound source is located on the object's left or right side. For this purpose simulations were run for a source positioned at an azimuthal angle of  $90^\circ$  and positioned on the opposite side at an azimuthal angle of  $270^\circ$ . In each case the angle of elevation was  $0^\circ$ . From the simulation results one can conclude that the head model is symmetric and numerical calculations can be limited to the half space bounded by the middle plane.

System response pick up points were situated inside the pinna at the entries into the aural canal. The pick up points were located in the place where the measuring microphones had been located during the measurement of HRTF. An experiment was performed in order to find out if a slight change in the location of a reception point affects the result of numerical calculations. For this purpose another mesh of reception points was introduced into the model. The external area was removed by about 1 mm from the original area. It became apparent that such shift of the response pick up points has no influence on the results of numerical calculations. Also no significant changes in the response depending on the location of a point on the mesh of reception points were found.

It was tested whether the location of response pick up points outside the auricular concha affects the result of simulation. For this purpose the response pick points were located opposite the entrance to the aural canal at a distance of about 13 mm from the original response reception area. Figures 6 and 7 show the results of simulations depending on the location of response pick up points. The response obtained for the points situated outside the pinna is clearly shifted downwards relative to the response for the points located inside the pinna. Differences occur practically in the whole investigated

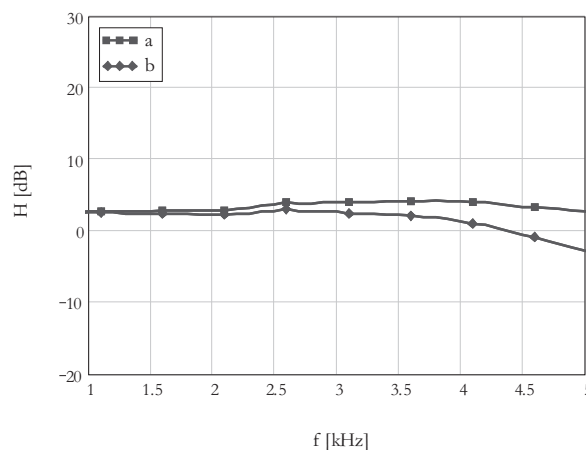


Fig. 6. Comparison of model responses for response pick up points located inside pinna (a) and outside pinna (b). Ipsilateral ear.

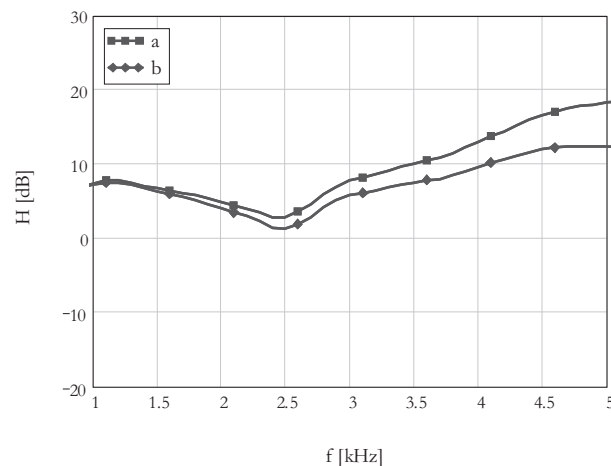


Fig. 7. Comparison of model response for response pick up points located inside pinna (a) and outside pinna (b). Contralateral ear.

frequency range, but significant differences occur above the frequency of 3–3.5 kHz. It is also observed that as the frequency increases so does the difference in the course of the responses. For the frequency of 3 kHz the difference is about 2 dB while for the frequency of 5 kHz the difference amounts to about 6 dB. The results obtained in this experiment confirm the literature reports according to which the pinna has the strongest influence on the sound frequency response above the frequency of about 3.5 kHz [15].

### 3. Surface acoustic impedance

It is necessary to know the acoustic impedance of the Neumann KU 100 head phantom since the model of this device is used for the numerical calculation of HRTE. Therefore a measurement must be performed to determine the value of this parameter [18].

The measurement was performed using the method based on the standing wave ratio [27]. In order to perform such a measurement one must have a material specimen whose shape allows it to be placed in a specimen grip. But the only specimen available during measurements is a specimen being part of the device. Since the separation of a piece suitable for measurement is bound with irreparable damage to the device the measurement was made without using a specimen grip. This was done by putting a flat area of the device against the impedance pipe's edge. Since the flat surface has the shape of a square with its side not exceeding 70 mm, the measurement was made using an impedance pipe 30 mm in diameter. The specimen cannot be put against a pipe 100 mm in diameter because of leakage which makes the measurement impossible. Therefore measurements were performed for a frequency in a range of 800–6300 Hz in 1/3-octave bands. In order to increase the system's tightness the outer part of the pipe-specimen connection was coated with silicone.

The results of measurements are presented in the figures above. Figure 8 shows the respective modulus and the acoustic impedance phase of the KU 100. One should note the shape and values of the particular frequency responses. The impedance modulus value oscillates around a certain average while the variability of the phase is slight – the phase practically has the value  $-\pi/2$  in the whole investigated range. Thus one can say that the acoustic impedance of the material from which the KU 100 is made has a compliance character. Although it is not a typical compliance graph the approximation seems to be justified. The reflection coefficient modulus of the KU 100 is close to 1 in the whole investigated frequency range. This result is similar as for skin.

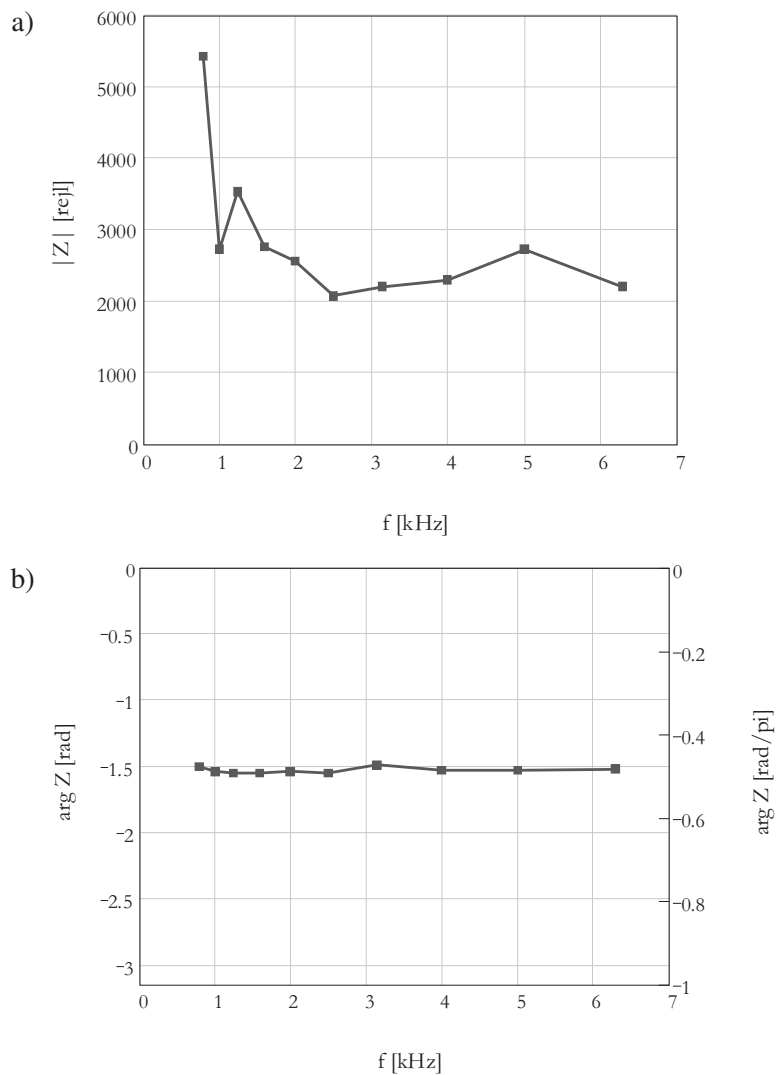


Fig. 8. Acoustic impedance of KU 100 a) modulus b) phase.

The KU 100's pinna is made from a different material than the other components. Therefore one can assume that the pinna's acoustic impedance is different than that of the other components. Nevertheless, because of the small dimensions of the pinna it was impossible to carry out acoustic impedance measurements. Since the pinna affects most the shape of the acoustic signal spectrum one can expect that if homogeneous boundary conditions are applied to the whole modelled area this may introduce a significant error. Therefore in further calculations one should consider carrying out a simulation for a model without any impedance boundary conditions, especially without any assigned impedance boundary conditions on the surface mapping the ear.

#### 4. Numerical calculation of HRTF

The properties of the acoustic field inside or outside the modelled area depend on its geometry and boundary conditions. In this paper the head-related transfer function was determined by the Boundary Element Method (BEM). In this method three kinds of boundary conditions for the Helmholtz equation can be distinguished: the Dirichlet boundary condition for acoustic pressure, the Neumann boundary condition for acoustic velocity and the Robin boundary condition specifying the dependence between acoustic pressure and velocity on the edge of the modelled area in the form of acoustic impedance [3, 8]. The problem to be solved consists in investigating the effect of a structure having a certain geometric shape on the propagation of the acoustic wave. Therefore thanks to the Neumann boundary conditions it will be possible to investigate the problem for the rigid model. In this case, assigned velocity  $v = 0$ . In order to investigate the influence of the material from which the real object is made one should apply the Robin boundary conditions, assigning an acoustic impedance consistent with the obtained measurement results.

The problem of determining the stationary acoustic field generated by a surface source boils down to solving the Helmholtz equation [7]

$$\Delta\Phi + k^2\Phi = 0, \quad (8)$$

where  $\Phi$  – the acoustic potential,  $k$  – the wave number.

The Neumann boundary condition can be written as

$$-\left. \frac{\partial\Phi}{\partial n} \right|_S = v_n(\xi), \quad \xi \in S, \quad (9)$$

where  $S$  – the structure's surface,  $n$  – a normal directed outward of the structure,  $\xi$  – a point on surface  $S$ ,  $v$  – acoustic velocity.

The Robin boundary condition can be written as

$$j\omega\rho_0\Phi|_S = Z(\xi)v_n(\xi), \quad \xi \in S, \quad (10)$$

where  $Z$  – the structure's surface acoustic impedance,  $\rho_0$  – air density.

HRTF contain information about a change in the sound spectrum as well as information about ILD and ITD. The interaural time difference can be easily mathematically

calculated from the geometric parameters of the investigated object whereas changes in the shape of the spectrum and the interaural differences in the sound level are more difficult to determine. The primary aim of the numerical calculation of HRTF is to determine changes in the sound spectrum. The secondary aim is to determine the proportion between the sounds reaching the individual ears.

The boundary element method is in two basic versions: direct BEM (DBEM) and indirect BEM (IBEM) [1]. In this work the IBEM method has been chosen, because for the model which consist of around twenty thousand elements this method is more effective. The unknown in IBEM method is the acoustic pressure jump or the acoustic velocity jump. Pressure difference  $\mu$  between the inner and outer side of surface  $S$  is called a pressure jump or the density of distribution of dipole sources. The difference in the normal derivatives of pressure  $\sigma$  between the outer and inner side of surface  $S$  is associated with an acoustic velocity jump and it is called the density of distribution of point sources (Fig. 9).

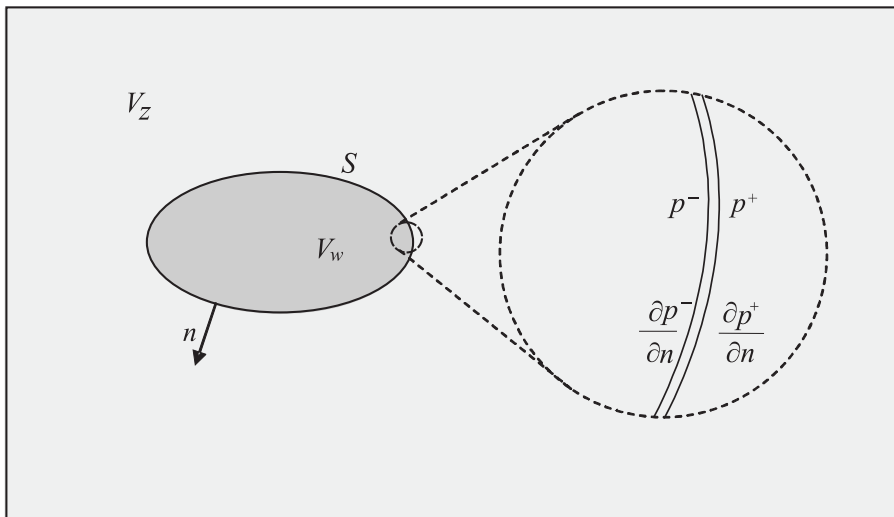


Fig. 9. Discontinuity of acoustic pressure and acoustic pressure derivative [16].

The distribution of density of dipole sources and the distribution of density of point sources are determined on the boundary element mesh. The distributions have no direct physical meaning and acoustic pressure is calculated from the following relation:

$$\int_S \left( \mu(\xi) \cdot \frac{\partial G(x, \xi)}{\partial n_\xi} - \sigma(\xi) \cdot G(x, \xi) \right) dS(\xi) = p(x), \quad (11)$$

where  $\mu = p^+ - p^-$  – the density of distribution of dipole sources on surface  $S$ ,  $\sigma = \partial p^+ / \partial n - \partial p^- / \partial n$  – the density of distribution of point sources on surface  $S$ ,  $\xi$  and  $x$  denote the point on the surface  $S$  and outside of the surface, respectively.

Surface  $S$  is divided into smaller parts depending on the assigned boundary conditions. Surface  $S_1$ , to which the Dirichlet boundary condition is assigned, will be neglected in further considerations since there are no surfaces with this boundary condition in the model. The Neumann boundary condition in the form:  $\partial p/\partial n = -j\rho_0\omega\bar{v}_n$  is assigned to surface  $S_2$ . In the modelled structure the surface remains rigid and so the assigned acoustic velocity is zero whereby normal derivative  $\partial p/\partial n = 0$ . Surface  $S_3$  is a surface to which the Robin boundary condition, i.e. acoustic impedance, is assigned. For surface  $S_3$  relation:  $z\partial p/\partial n + jkp = 0$  at  $z = Z/Z_0$  holds.

The unknowns:  $\sigma(\xi)$  and  $\mu(\xi)$  are calculated depending on the type of applied boundary condition. For the Neumann boundary condition acoustic pressure and velocity jumps on surface  $S_2$  assume the respective values:  $\sigma = 0$ ,  $\mu \neq 0$ . For the Robin boundary condition acoustic pressure and velocity jumps on surface  $S_3$  assume the values:  $z\sigma + jk\mu = 0$  and  $\mu \neq 0$ .

Thus for a zero acoustic velocity value on the area's edge one gets:

$$\eta \in S_2 \Rightarrow \frac{\partial p(\eta)}{\partial n} = 0, \quad (12)$$

$$\int_{S_2} \mu(\xi) \frac{\partial^2 G(\xi, \eta)}{\partial n_\xi \partial n_\eta} dS_2(\xi) + \int_{S_3} \mu(\xi) \left( z_\xi \frac{\partial^2 G(\xi, \eta)}{\partial n_\xi \partial n_\eta} + jk \frac{\partial G(\xi, \eta)}{\partial n_\eta} \right) dS_3(\xi) = 0. \quad (13)$$

For a constant acoustic impedance on the area's boundary one gets:

$$\eta \in S_3 \Rightarrow z_\eta \frac{\partial p(\eta)}{\partial n} + jkp(\eta) = 0, \quad (14)$$

$$z_\eta \left[ \int_{S_2} \mu(\xi) \frac{\partial^2 G(\xi, \eta)}{\partial n_\xi \partial n_\eta} dS_2(\xi) + \int_{S_3} \mu(\xi) \left( z_\xi \frac{\partial^2 G(\xi, \eta)}{\partial n_\xi \partial n_\eta} + jk \frac{\partial G(\xi, \eta)}{\partial n_\eta} \right) dS_3(\xi) \right] + jk \left[ \int_{S_2} \mu(\xi) \frac{\partial G(\xi, \eta)}{\partial n_\xi} dS_2(\xi) + \int_{S_3} \mu(\xi) \left( z_\xi \frac{\partial G(\xi, \eta)}{\partial n_\xi} + jkG(\xi, \eta) \right) dS_3(\xi) \right] = 0. \quad (15)$$

In relations (13) and (15) the integrals containing singular points are calculated in terms of their principal values.

Taking into account the considerations discussed in [3], it was determined that IBEM calculations should be performed for quadratures 5-2-1. The respective numbers represent the order of a quadrature for a nearby area (a distance shorter than 2 elements), a mid area (a distance shorter than 5 elements) and a distant area (a distance of 5 and more elements). For the parameters set as above calculation errors are only the result of shape approximation errors. In order to verify the assumed orders of quadratures several simulations were run for different quadrature values. The results of simulations do not depend on the order of the quadratures used. Also for the model with assigned impedance boundary conditions the order of quadratures was found to have no influence on calculation results. Since there are no significant differences in the duration of numerical computations for the quadratures: 5-2-1 and 2-2-2, the 5-2-1 quadrature order was used in further considerations.

The final parameter which needs to be set is the frequency resolution of the numerical calculation of the system response. According to literature reports HRIR should be at least 128 samples long [10], which at a sampling frequency of 44.1 kHz gives a frequency analysis resolution (for the FFT algorithm) of about 350 Hz. Since simulation results will be compared with the results of the Fourier transform for which the distribution of points in the frequency domain is linear it was assumed that the distribution of points in the frequency domain will be linear also for the simulations. On the basis of an analysis of preliminary simulation results it was determined that the frequency resolution should be not higher than 100 Hz. Ultimately the frequency resolution was set at 50 Hz. This corresponds to a situation for which the impulse response has the length of about 880 samples, i.e. much more than 128 samples.

## 5. Comparison of results

A system for measuring HRTFs and measurements by means of this system were made in collaboration with the Institute of Electronics at Łódź University of Technology [5, 20, 23, 28]. The HRTF measurement results are stored in the form of an impulse response [27]. In order to obtain a frequency response the impulse response is subjected to the Fourier transformation by means of the FFT algorithm. But the obtained curve is considerably nonuniform (Fig. 10). In order to make it possible to compare the measurement result with the simulation result, the former was subjected to averaging. This operation was performed using an average weighted with the Gaussian curve [14]. Each point of the averaged curve is determined from the value of a specified number of neighbouring points. Averaging is performed for each point  $i$  according to the following relations:

$$y'_i = \frac{\sum_{j=1}^n K \left( \frac{x_i - x_j}{b} \right) y_j}{\sum_{j=1}^n K \left( \frac{x_i - x_j}{b} \right)}, \quad (16)$$

where  $K(t) = 1/\sigma\sqrt{2\pi} \exp(-t^2/2 \cdot \sigma^2)$ ,  $b$  – the bandwidth,  $n$  – the number of points in the band,

$$1 \leq i, j \leq n.$$

The averaging method used is proper for graphs with points uniformly distributed along the X-axis. Since the results of the comparison are presented for a linear frequency scale, the adopted method of averaging is proper. On the other hand, the linear frequency scale was chosen in view of the linear distribution of the points yielded by FFT. Figure 10 shows the result of averaging the measurement results. Thanks to averaging, the graph is devoid of the irregularities due to the measurement method.

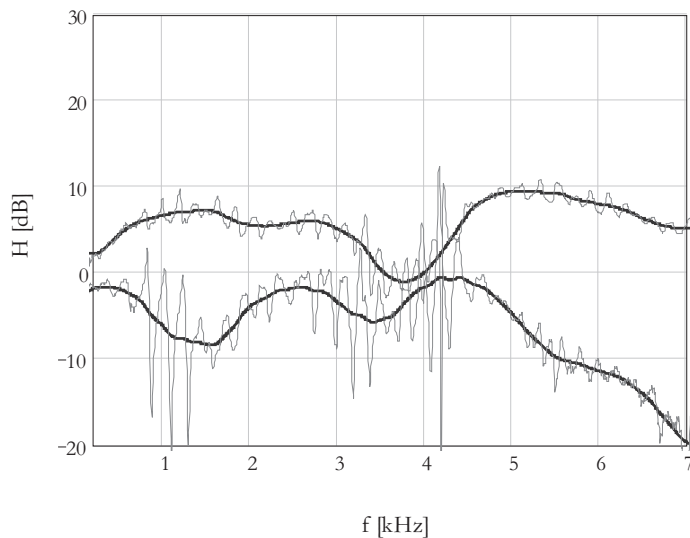


Fig. 10. Frequency response: fine line – FFT result, heavy line – averaged FFT result.

The results are compared in a frequency range of 200 Hz – 7 kHz. The lower limit of the compared frequency range is determined by the measuring device constraints and it is equal to the limit frequency. The upper limit of the compared area is determined by the constraints of the model used for the numerical calculation of the head-related transfer function. The frequency of 7 kHz is situated slightly higher than the value for which the condition of four acoustic wavelengths per element linear dimension is satisfied for all the model elements.

Figure 11 show HRTF measurement and numerical calculation results, including the results for selected (the most characteristic) points in the space surrounding the listener. Figures assigned by a) show the measurement and simulation results for the ipsilateral ear (located closer to the sound source) while the figures b) show the results for the contralateral ear (located further away from the sound source). There are four graphs in each diagram. The particular letters in each diagram represent the following cases: i – the measurement result, ii – the result of simulations without impedance boundary

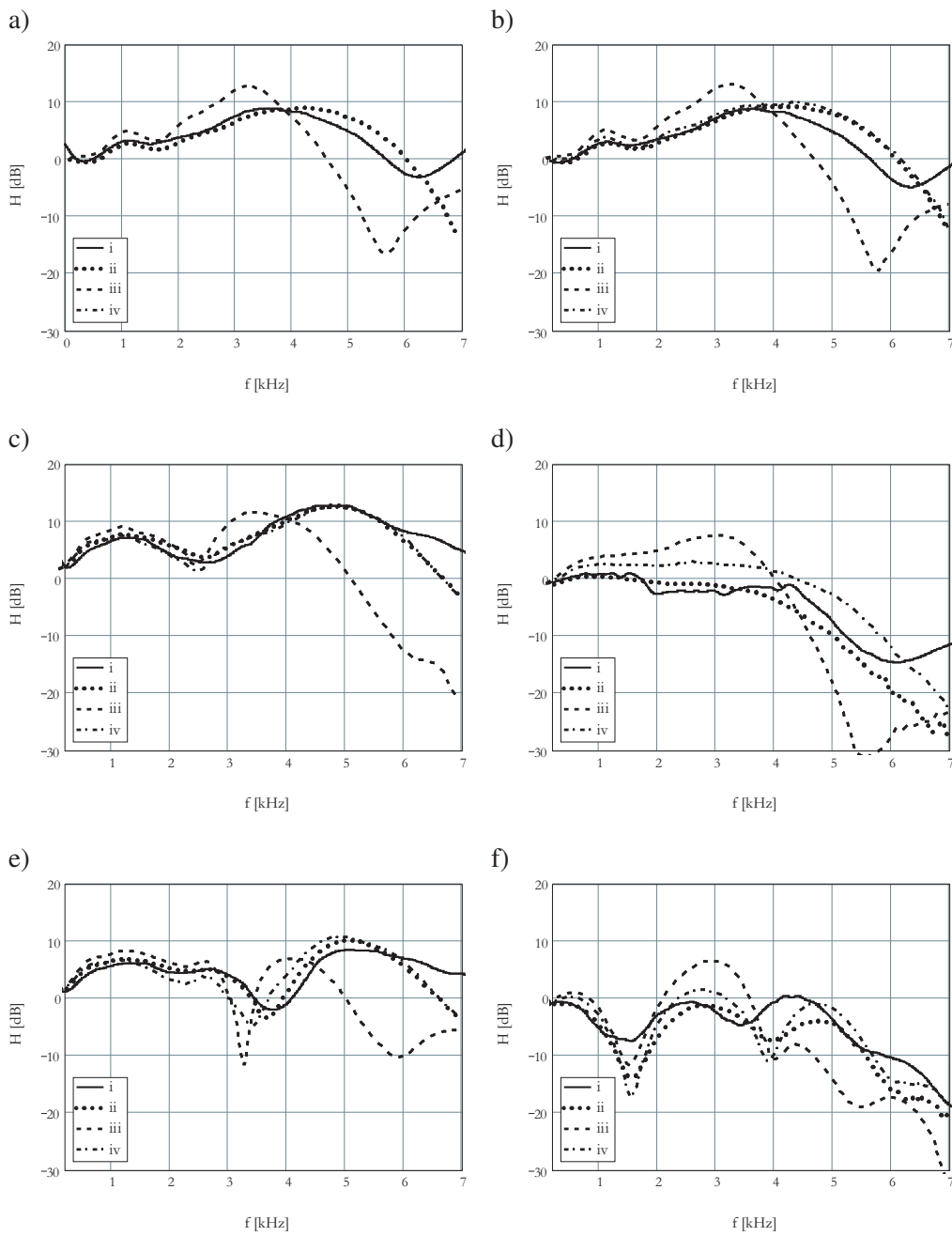


Fig. 11. Measurement and simulation results: a) azimuth  $0^\circ$ , elevation  $0^\circ$ , ipsilateral ear, b) azimuth  $0^\circ$ , elevation  $0^\circ$ , contralateral ear, c) azimuth  $90^\circ$ , elevation  $0^\circ$ , ipsilateral ear, d) azimuth  $90^\circ$ , elevation  $0^\circ$ , contralateral ear, e) azimuth  $120^\circ$ , elevation  $0^\circ$ , ipsilateral ear, f) azimuth  $120^\circ$ , elevation  $0^\circ$ , contralateral ear. Detailed description of symbols in text.

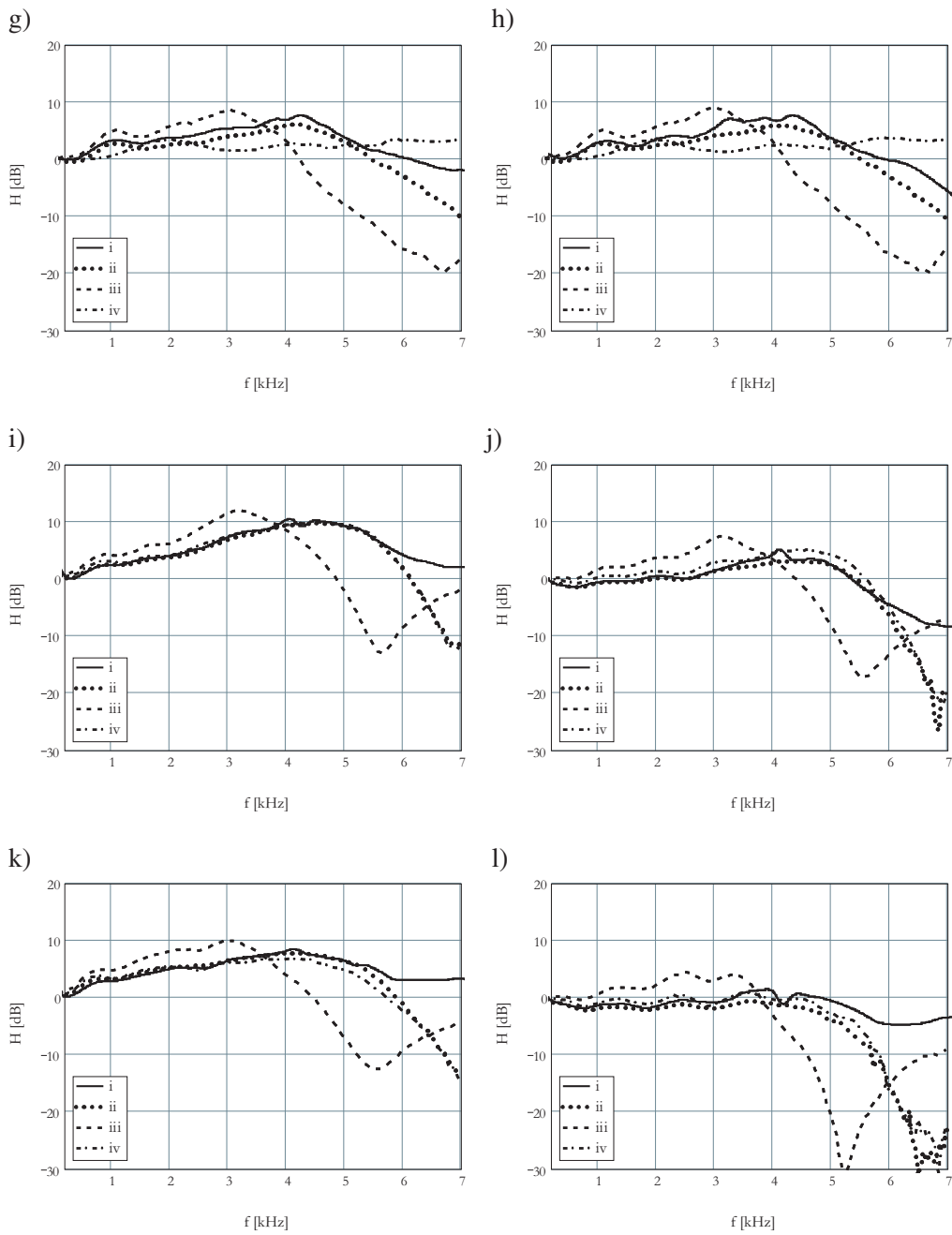


Fig. 11. [Cont.] Measurement and simulation results: g) azimuth  $180^\circ$ , elevation  $0^\circ$ , ipsilateral ear, h) azimuth  $180^\circ$ , elevation  $0^\circ$ , contralateral ear, i) azimuth  $30^\circ$ , elevation  $60^\circ$ , ipsilateral ear, j) azimuth  $30^\circ$ , elevation  $60^\circ$ , contralateral ear, k) azimuth  $120^\circ$ , elevation  $60^\circ$ , ipsilateral ear, l) azimuth  $120^\circ$ , elevation  $60^\circ$ , contralateral ear. Detailed description of symbols in text.

conditions (the rigid model), iii – the result of simulations with impedance boundary conditions in the whole modelled area, iv – the result of simulations with impedance boundary conditions in whole modelled area except for the pinnas, for which the same boundary condition as for the rigid model was assumed.

## 6. Conclusions

The head-related transfer functions measured for artificial head KU 100 are the reference with which computer simulation results are compared. Hence it is essential to know the accuracy of the measurement results. It is difficult to evaluate this accuracy since precise HRTF graphs are not known whereby it is impossible to estimate the measuring error. Measurement accuracy can be evaluated on the basis of subjective assessments of auralization combined with the use of measurement results. Preliminary comparative tests carried out at Łódź University of Technology indicate that the tested persons much better localize sounds processed with measured HRTFs than with HRTFs taken from other databases. Therefore one can conclude that the results of measurements are correct and they can be used as the basis for verifying the results of numerical calculations of HRTFs.

The simulation results for the rigid model are very close to the measurement results from the frequency of about 200 Hz to 5.5–6.0 kHz. The differences in the plots are not greater than 2 dB. Above the frequency of 6 kHz the simulation values are greater than the measured ones, but the divergences are not larger than 10 dB.

The results of simulations with impedance boundary conditions assigned to the whole modelled area are qualitatively consistent but quantitatively divergent. The frequencies at which the maxima and minima of the responses occur are similar, whereas the differences in the levels between the maxima and the minima are larger than for the responses determined using the rigid model. The difference in the values on the average amount to about 10 dB. One can notice that the maximum of the response for both the ipsilateral ear and the contralateral ear occurs at a frequency of about 3.5 kHz. Thus the latter is a frequency above which the influence of the pinna on the acoustic wave spectral response begins to increase. On this basis several simulations with boundary conditions assigned to the whole model area, except for the pinnas (the latter remained rigid), were carried out.

The results of simulations with impedance boundary conditions assigned to the whole area, except for the pinnas, are in agreement with the measurement results up to a frequency of about 6 kHz. In the whole investigated frequency range the results of numerical determination of the functions are close to the results obtained for the rigid model. On the other hand, the calculated values are close to the values obtained for the model with acoustic impedance assigned to the whole model up to a frequency of about 3-3.5 kHz. Above this frequency the results differ considerably. Thus one can say that despite the similarity of the materials from which the head and the pinnas are made, the acoustic impedances of the two materials are significantly different. Hence one can

conclude that if proper boundary conditions are assigned to the areas of the pinnas, the simulation results will be closer to the measurement results.

Several simulations for different boundary conditions were run for the head area and the areas of the pinnas. In the case of the head area, the measured acoustic impedance was used while the impedance value found in the literature [9] was used for the areas of the pinnas. Despite this, the obtained results do not significantly differ from the simulation results in the case of which no impedance boundary conditions were assigned to the pinnas. The values reported in the literature are limited to the acoustic impedance modulus while the measurement results indicate that the phase shift is more important for the results of simulations.

To recapitulate, contrary to expectations the assignment of impedance boundary conditions to the whole modelled area does not improve the results of simulations. Better results are obtained if a model with impedance boundary conditions assigned to the whole modelled area, except for the pinnas (which remain rigid), is used in the simulations. The best results are obtained for a totally rigid model. Hence one can conclude that the course of HRTF is most affected by the geometric shape of the model while acoustic impedance to a certain extent modifies the range of changes in the shape of the response, but it does not change the frequencies at which the maxima and minima of the responses occur. The application of impedance boundary conditions to the area for which the acoustic impedance was measured changes the results of simulation. It seems that the use of a proper acoustic impedance value for the pinnas could bring the simulation results significantly closer to the measured values. The divergence of the results above 3.5 kHz confirms the literature reports indicating that the pinna has the strongest influence on the modification of the acoustic signal spectrum in a frequency range of 3.5-5 kHz [17].

The results obtained by calculation are similar to the measurements results. Between calculation and measurements results better agreement has been obtained in comparison to other papers, e.g. [11, 12]. It is possible to use the presented model to further research about the influence of such parameters as the pinna shape, the head circumference and other boundary impedance conditions on HRTF.

## References

- [1] ALI A., RAJAKUMAR C., *The Boundary Element Method. Application in Sound and Vibration*, A.A. Balkema Publishers, Leiden 2004.
- [2] BLAUERT J., *Spatial hearing*, MIT Press, Cambridge, Massachusetts 1997.
- [3] BOLEJKO R., *Numerical modelling of acoustic field inside and outside bounded areas with impedance boundary conditions taken into account* [in Polish], Ph.D. thesis, Wrocław University of Technology, Wrocław 2004.
- [4] BRAŃSKI A., *Analysis of acoustic parameters of boundary problems* [in Polish], Wydawnictwo Wyższej Szkoły Pedagogicznej, Rzeszów 2001.

- 
- [5] BUJACZ M., STRUMIŁŁO P., *Stereophonic representation of virtual 3D scenes – a simulated mobility for the blind*, [in:] *New Trends in Audio and Video*, Vol. 1, Białystok 2006.
- [6] CHENG C.I., WAKEFIELD G.H., *Introduction to head-related transfer functions (HRTFs): Representations of HRTFs in time, frequency, and space*, *Journal of the Audio Engineering Society*, **49**, 231–249 (2001).
- [7] DOBRUCKI A.B., *Electroacoustic transducers* [in Polish], Wydawnictwa Naukowo-Techniczne, Warszawa 2006.
- [8] VON ESTORFF O. [Ed.], *Boundary Elements in Acoustics*, WIT Press, Southampton 2000.
- [9] GABRIEL K., PETRIE S., *Ultrasonic absorption in rubber filled epoxies*, ANTEC 2000 *Plastics: The Magical Solution*, Volume 2: *Materials*, Society of Plastics Engineers, Knovel 2001.
- [10] HORBACH U., KARAMUSTAFAGLU A., PELLEGRINI R., MACKENSEN P., THEILE G., *Design and Applications of a Data-based Auralization System for Surround Sound*, Presented at the 106th AES Convention, Munich 1999.
- [11] KATZ B.F.G., *Boundary element method calculation of individual head-related transfer function. I. Rigid model calculation*, *Journal of the Acoustical Society of America*, **110**, 2440–2448 (2001).
- [12] KATZ B.F.G., *Boundary element method calculation of individual head-related transfer function. II. Impedance effects and comparisons to real measurements*, *Journal of the Acoustical Society of America*, **110**, 2449–2455 (2001).
- [13] KIN M.J., PLASKOTA P., *Reproduction of acoustic atmosphere in music recordings, using dummy head* (in Polish), [in:] *Proceedings of the 11th International Symposium the Art of Sound Engineering*, Cracow 2005.
- [14] MATHSOFT ENGINEERING & EDUCATION, *Mathcad User's Guide*, Cambridge 2005).
- [15] MOORE B.C.J., *An Introduction to the Psychology of Hearing*, 4th Ed., Academic, San Diego 1997.
- [16] NUMERICAL INTEGRATION TECHNOLOGIES, *Synoise Theoretical Manual*, NIT, Leuven 1993.
- [17] PLASKOTA P., *Conception of numerical model of human head for HRTF numerical calculation* [in Polish], In: *Proceedings of the 10th Conference "New Trends in Audio and Video"*, Wrocław 2004.
- [18] PLASKOTA P., *Measurement of acoustical impedance of human skin*, [in:] *The 6th European Conference on Noise Control EURONOISE 2006*, *Proceedings*, Acoustical Society of Finland, Finland, Tampere 2006.
- [19] PLASKOTA P., *Numerical calculation of HRTF – head model* [in Polish], [in:] *Proceedings of the 52nd Open Seminar on Acoustics*, Poznań–Wągrowiec 2005.
- [20] PLASKOTA P., *Evaluation of microphone parameters for HRTF measurement* [in Polish], [in:] *Proceedings of the 10th International Symposium the Art of Sound Engineering*, Wrocław 2003.
- [21] PLASKOTA P., DOBRUCKI A. B., *Numerical head model for HRTF simulation*, In: *Proceedings of the 118th AES Convention*, Preprint 6510, Barcelona 2005.
- [22] PLASKOTA P., DOBRUCKI A. B., *Ambience reproduction with dummy head utilisation* [in Polish], [in:] *Proceedings of the 11th International Symposium the Art of Sound Engineering*, Cracow 2005.
- [23] PLASKOTA P., DOBRUCKI A. B., *Selected problems of HRTF measurement* [in Polish], [in:] *Metrology Congress*, Wrocław 2004.
- [24] PLASKOTA P., KIN M. J., *The use of HRTF in sound recordings* [in Polish], [in:] *Proceedings of the 9th Conference "New Trends in Audio and Video"*, Warszawa 2002.

- [25] PLASKOTA P., PRUCHNICKI P., *Practical aspects of using HRTF measuring device*, Archives of Acoustics, **31**, 439–444 (2006).
- [26] PLASKOTA P., WASILEWSKI M., KIN M. J., *The use of Head-Related Transfer Functions in auralization of sound recordings* [in Polish], [in:] Proceedings of the 10th International Symposium the Art of Sound Engineering, Wrocław 2003.
- [27] PN-EN ISO 10534-1:2004, *Acoustics – Determination of sound absorption coefficient and acoustic impedance in impedance tubes– Part 1: Method using standing wave ratio* [in Polish], PKN, Warsaw 2004.
- [28] PRUCHNICKI P., PLASKOTA P., *HRTF Automatic measuring system*, Presented at the 53 Open Seminar on Acoustics, Zakopane 2006.